Digital Discovery

Accepted Manuscript

This article can be cited before page numbers have been issued, to do this please use: D. Bincoletto and J. Kottmann, *Digital Discovery*, 2025, DOI: 10.1039/D5DD00251F.

ROYAL SOCIETY OF CHEMISTRY

rsc.li/digitaldiscovery

View Article Online
DOI: 10.1039/D5DD00251F

Journal Name

ARTICLE TYPE

Cite this: DOI: 00.0000/xxxxxxxxxx

A Physics-Informed Measurement Protocol for Expectation Values of Fermionic Observables

Davide Bincoletto,[a] and Jakob S. Kottmann*[a,b]

Received Date
Accepted Date

DOI: 00.0000/xxxxxxxxxx

A central roadblock in the realization of Variational Quantum Eigensolvers on quantum hardware is the high overhead associated with measurement repetitions, which hampers the simulation of complex systems, such as mid- and large-sized molecules. We propose a novel measurement protocol which relies on computing an approximation of the Hamiltonian expectation value. It involves an iterative procedure that measures easily accessible operator groups in different Fermionic bases. The measured elements are defined by the Hard-Core Bosonic approximation, which encode electron-pair annihilation and creation operators. These can be decomposed into three self-commuting groups to measure simultaneously. Applied to molecular systems, the method achieves a reduction of 30% to 80% in the number of measurement and gates depth in the measuring circuits compared to state-of-the-art methods. This provides a scalable and cheap measurement protocol, advancing the application of variational approaches for simulating physical systems.

1 Introduction

The Variational Quantum Eigensolver (VQE) [1,2] are often considered promising candidates for practical applicable quantum algorithms. [3–6] One of the main roadblocks for successful applications is the significant overhead of circuit executions (shots) to estimate a single expectation value of a given Hamiltonian. Even outside the scope of variational algorithms, this bottleneck will still be present, as for example reduced density matrices remain a crucial observable for many applications. [7,8] Consider the electronic structure problem of quantum chemistry, which aims to find the eigenstates of many-electron systems. Measuring the Hamiltonian in second quantization reduces to measuring the terms:

$$\langle H \rangle = \sum_{kl}^{N} h_{kl} \langle a_k^\dagger a_l \rangle + \frac{1}{2} \sum_{klmn}^{N} g_{klmn} \langle a_k^\dagger a_l^\dagger a_n a_m \rangle \tag{1}$$

with N being the number of spin-orbitals in the system. In this form, $\mathcal{O}(N^4)$ types of individual shots have to be realized in order to estimate the full expectation value. On noisy hardware, but also with respect to estimated runtimes, this overhead is currently preventing practical demonstrations of VQEs already on moderate-sized systems. [9,10] A class of strategies out of this dilemma are so-called grouping methods that identify commuting cliques in the individual parts of the Hamiltonian which can then be measured simultaneously – therefore reducing the overhead from $\mathcal{O}(N^4)$ to the number of commuting cliques. As finding the optimal cliques is an NP-hard problem, various heuristics based on qubit [11–13] and Fermionic [14–16] representations have been proposed. So far, these methods focus on (near-) exactly decompositions of the full Hamiltonian without taking advantage of physical approximations tailored to the system of interest. Furthermore, there are other methods which consider adaptive procedures. [17–19]

Our work presents a method for reducing measurements overhead by exploiting the structure of the given electronic instance. The procedure aims to approximate the expectation value of the Hamiltonian with respect to a specific target state (in this case, the ground-state of the electronic system). The goal is to heuristically leverage the structure of the quantum state at hand instead of aiming to partition the Hamiltonian into commuting cliques, which can become computationally expensive and often comes with an increased overhead in circuit depth. We show that the proposed methods achieves significant reductions in measurement types as well as in circuit overheads.

2 Central Ideal

The $O(N^4)$ overhead described above can be eliminated by approximating the electronic system as a collection of spin-paired quasi-particles, called Hard-Core Bosons (HCB). [20] This approximation allows the Hamiltonian to be divided into exactly three commuting groups, regardless of the system size. However, this approach often falls short in accurately describing electronic systems, particularly those where quantum computers are expected to provide significant improvements in precision. Therefore,

[a] Institute for Computer Science, University of Augsburg; E-mail: jakob.kottmann@uni-a.de
[b] Centre for Advanced Analytics and Predictive Sciences, University of Augsburg.

View Article Online
DOI: 10.1039/D5DD00251F

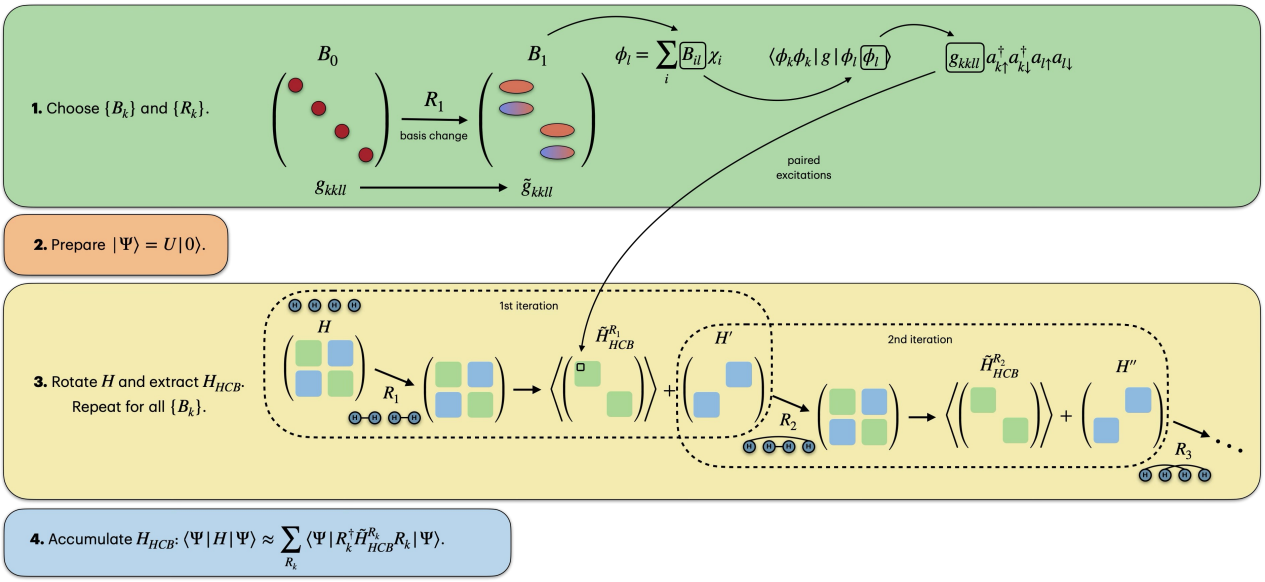

Fig. 1 Illustration of the measurement routine used in this article leveraging HCB approximation and basis rotations. The general procedure is applied to hydrogenic systems like H_4 (depicted in the Figure), H_6 and H_8. Here diagonal and off-diagonal matrix elements (green and blue) are used to represent HCB and residual Hamiltonian elements.

limiting variational algorithms to HCB Hamiltonians is not a viable solution. The core idea of this research is to leverage the straightforward grouping of HCB Hamiltonians and combine them with orbital rotations to switch between different frames of the approximation in order to iteratively improve the estimate of the expectation values at hand. At this point, it is important to note that the electronic states of interest are not formulated using the HCB approximation.

3 Technical Background

In the following we will introduce Hard-core Bosonic Hamiltonians in the specific (non-compressed) form necessary for the measurement protocols developed in this work, followed by a recap of orbital rotations and their implementation as quantum circuits. The experienced reader might skip this section.

3.1 Hard-Core Boson Hamiltonian

In the Hard-Core Boson approximation (see for example Ref. 20 for an application for VQEs) spin-paired-electrons are treated as quasi-particles, occupying the spatial orbitals. Applied to an electronic system, this breaks the invariance of the Hamiltonian with respect to orbital rotations, meaning that different choices of spatial orbitals lead to different approximations. In 21 this was used to approximate electronic eigenstates as linear combinations over HCB states in different orbital "frames" which served as the initial motivation for this work. The approximation can be formulated as

$$H_{\mathrm{HCB}} = \sum_k \alpha_k + \sum_{kl}(\beta_{kl} + \gamma_{kl} + \delta_{kl}) \tag{2}$$

where

$$\alpha_k = \sum_\sigma h_{kk}a^\dagger_{k\sigma}a_{k\sigma} = \sum_\sigma h_{kk}n_{k\sigma},$$
$$\beta_{kl} = \sum_{\sigma,\sigma'} g_{kkll}a^\dagger_{k\sigma}a^\dagger_{k\sigma'}a_{l\sigma'}a_{l\sigma}$$
$$\gamma_{kl} = \sum_{\sigma,\sigma'} g_{kllk}a^\dagger_{k\sigma}a^\dagger_{l\sigma'}a_{l\sigma'}a_{k\sigma} = \sum_{\sigma,\sigma'} g_{kllk}n_{k\sigma}n_{l\sigma'}$$
$$\delta_{kl} = \sum_{\sigma,\sigma'} g_{klkl}a^\dagger_{k\sigma}a^\dagger_{l\sigma'}a_{k\sigma'}a_{l\sigma} \tag{3}$$

are the operators that encode spin-paired creation and annihilation. And the residual Hamiltonian is $H_{\mathrm{res}} = H - H_{\mathrm{HCB}}$. The resulting HCB Hamiltonian, once mapped into Pauli operators, naturally decomposes into three commuting groups: $\{I_0, Z_0, Z_1, Z_0Z_1, \ldots\}$, $\{Y_0X_1X_2Y_3, X_0Y_1Y_2X_3, Y_0X_1X_4Y_5, \ldots\}$ and $\{Y_0Y_1X_2X_3, X_0X_1Y_2Y_3, Y_0Y_1X_4X_5, \ldots\}$. Namely, α_k and γ_{kl} parse into the first group, and β_{kl} and δ_{kl} parse in the second and third groups. This makes it possible to do measurement on multiple elements at the same time, highly reducing the computational overhead. Note that, the formulation used here differs from other works[20,22–24] that use a compressed representation (single qubit for a spatial orbital) – this is however only possible if the quantum state is also in the HCB approximation, which is not the case here.
Since the standard measurement on quantum computers consists of reading out the classical bit values of the qubits (this corresponds to measuring in the Z-basis), we need to transform all the other Pauli operators in the Hamiltonian. This means finding a

View Article Online
DOI: 10.1039/D5DD00251F

set of unitary operators such that

$$P_i^{(d)} \equiv P_i^z = U_i P_i U_i^\dagger \tag{4}$$

where $P_i^{(d)}$ is a diagonal matrix in the form of a tensor product consisting only of Pauli-Z and unit matrices. In this work, the unitary operators, or measurement circuits, were identified using the Sorted Insertion (SI) method, with an asymptotical scaling of $\mathcal{O}\left(N_q^2/\log(N_q)\right)$ in the number of 2-qubit entangling gates and single qubit rotations.[12,25] However, in principle, they can be further optimized by tailoring them to the three groups, as the Pauli string pattern exhibits repetition.

3.2 Orbital Rotation Operations

An orbital basis is a unitary $N \times N$ matrix B operating on the initial set of spatial orbitals. In order to rotate a basis we need to define a operation that preserves the electronic Hamiltonian structure. An effective 2D rotation (Givens rotation) acts as a proper basis change for consecutive orbitals. Thus, in order to rotate any orbital we can use a sequence of effective 2D rotations acting on the atomic orbital space. To illustrate, this is the matrix representation in the space of two spatial orbitals p and q:

$$R_{\{p,q\}}(\theta) \equiv R(\theta) = \begin{pmatrix} \cos(\theta/2) & \sin(\theta/2) \\ -\sin(\theta/2) & \cos(\theta/2) \end{pmatrix} \tag{5}$$

where θ is a free parameter. This operation is applied to the molecular integrals to define a global unitary transformation of the Hamiltonian operator. We will refer to this operation as orbital rotation.

Such an effective 2D rotation can be also represented as a quantum circuit, given the correspondence between atomic orbital space and qubit space.[26–28] In fact the unitary operator

$$U_{R_{\{p,q\}}}(\theta) \equiv U_R(\theta) = e^{\frac{\theta}{2}(a_{p\uparrow}^\dagger a_{q\uparrow} + a_{p\downarrow}^\dagger a_{q\downarrow} - \text{h.c.})}, \tag{6}$$

which acts on the qubit space, achieves the same result of an orbital rotation operation.[28] Here p and q represent the spatial orbitals affected by the rotation. Thus, analogously to the atomic orbital space, an orbital rotation operation in the qubit space is achieved with a sequence of $U_R(\theta)$. While the matrix representation is an $N \times N$ operation on the space of of N spatial orbitals, the circuit representation correspond to a $2^{2N} \times 2^{2N}$ transformation applied on the qubit register.

4 Detailed Description

The proposed method consists of four steps: a preprocessing phase (steps 1–2), performed once, a recursive phase (step 3), and a final phase (step 4), executed for each estimation of the expectation value of the whole Hamiltonian.

1. **Choose orbital bases $\mathscr{B} = \{B_k\}$.**

   The orbital bases are given as unitary $N \times N$ matrices which operates on the initial set of orbitals, called "reference orbitals". Note that they do not need to be "Hartree-Fock" orbitals, they merely define the reference for B_k. Each matrix in $\mathscr{B}$ is compiled into a orbital rotation operation forming the set $\mathscr{R} = \{R_k\} = \{U_{R_k}\}$ of rotation matrices and corresponding quantun circuits.

2. **Prepare the quantum state of interest.**

   This can be defined as

   $$|\Psi\rangle = U|0\rangle, \tag{7}$$

   where U is a quantum circuit, and $|0\rangle$ the quantum register. This is the state of which we aim to compute the expectation value.

3. **Iteratively approximate the expectation value of H**

   H is transformed into $H = \tilde{H}_{\text{HCB}}^{R_1} + H'$, with

   $$\tilde{H}_{\text{HCB}}^{R_1} = (R_1 H R_1^\dagger)_{\text{HCB}} \tag{8}$$

   $$H' = (R_1 H R_1^\dagger)_{\text{res}} \tag{9}$$

   An expectation value of $\tilde{H}_{\text{HCB}}^{R_1}$ can be estimated straightforwardly since all the terms can be collected into three commuting groups, as shown before. The error of this estimate is contained within the residual operator H' which can be recursively processed in the same way we did for H. Each cycle will take a new rotation operation from the set $\{R_1, R_2, R_3, ...\}$, rotate back in the original basis, rotate forward in the new basis and extract HCB and residual Hamiltonian.

4. **Accumulate all contributions**

   Finally, we have collected a series of expectation values that approximate the expectation value of the original Hamiltonian H.

   $$\langle\Psi|H|\Psi\rangle \approx \sum_{R_k \in \mathscr{R}} \langle\Psi|R_k^\dagger \tilde{H}_{\text{HCB}}^{R_k} R_k|\Psi\rangle \tag{10}$$

   The expectation value over the last constructed residual operator H' quantifies the error exactly. The approximation neglects this final residual.

The crucial point of the method is that an accurate approximation is bound to a correct choice of the orbital rotations, this is the heuristic part in step 1. In the following, we present two typical scenarios for practical applications, where we guess orbital bases based on the structure of the given electronic system and leverage concepts from Valence-Bond Theory. We further showcase some instances with randomly selected bases.

4.1 Numerical Results: Measurement Groups

To analyze and illustrate the method proposed above, we will consider two explicit scenarios. One uses the exact ground state and we will employ valence-bond based heuristics to generate the orbital rotations necessary in the first step of the method. In the second scenario we will illustrate co-design with existing circuit designs to generate the orbital rotations.

View Article Online
DOI: 10.1039/D5DD00251F

Scenario I: we make no assumption on the quantum circuit that produces the state. In order to run the simulations we computed the true ground-state through exact diagonalization. This ensures that all essential correlations are represented in the wavefunction of interest. For the rotation operations we leverage Valence-Bond Theory for chemical bonding construction[29] following some of our previous works.[21,28] For example, for a H_4 molecule arranged in a linear geometry we can define a graph identified by only paired edges, namely $G_1 = \{\{0,1\},\{2,3\}\}$:

$G_1 =$ 

Then, given a set of reference orbitals, we can associate one orbital rotation operation to each graph. In a minimal STO-3G atomic basis, G_1 corresponds to a rotation in a four orbitals space. By arranging the values in rows $\{0,1\},\{2,3\}$, corresponding to the graph nodes, the operation can be represented by the matrix (for $\theta = \frac{\pi}{2}$):

$$\begin{aligned} R_{G_1}\left(\frac{\pi}{2}\right) &= R_{\{\{0,1\},\{2,3\}\}}\left(\frac{\pi}{2}\right) = \\ &= R_{\{0,1\}}\left(\frac{\pi}{2}\right)\ R_{\{2,3\}}\left(\frac{\pi}{2}\right) = \\ &= \frac{1}{\sqrt{2}}\begin{pmatrix} 1 & 1 & 0 & 0 \\ -1 & 1 & 0 & 0 \\ 0 & 0 & 1 & 1 \\ 0 & 0 & -1 & 1 \end{pmatrix} \end{aligned} \tag{11}$$

The coefficients show that the orbitals are now in an equal superposition, thus, we can interpret the first row as a bonding molecular orbital between atomic orbitals 0 and 1 and the second row as an anti-bonding molecular orbital, likewise for the third and fourth rows. Therefore, the rotation operation R_{G_1} is the transformation from the set of reference orbitals B_0, where atomic orbitals have no interaction among them, to the orbital basis B_1, where orbital pairs $\{0,1\},\{2,3\}$ are delocalized into bonding and anti-bonding motifs. The graph G_1 corresponds to $p,q = 0,1$ and $p,q = 2,3$. We will represent such circuits graphically as

$U_{R_{G_1}}\left(\frac{\pi}{2}\right) \equiv$ 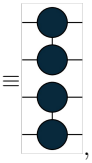 , (12)

where the lines represent spatial orbitals (and therefore 2-qubits in most encodings). The corresponding unitary operators are:

$$\begin{aligned} U_{R_{G_1}} &= U_{R_{\{\{0,1\},\{2,3\}\}}}\left(\frac{\pi}{2}\right) = \\ &= U_{R_{\{0,1\}}}\left(\frac{\pi}{2}\right)\ U_{R_{\{2,3\}}}\left(\frac{\pi}{2}\right) = \\ &= e^{\frac{\pi}{4}\left(a^\dagger_{0\uparrow}a_{0\uparrow} + a^\dagger_{1\downarrow}a_{1\downarrow} - \text{h.c.}\right)}\ e^{\frac{\pi}{4}\left(a^\dagger_{2\uparrow}a_{2\uparrow} + a^\dagger_{3\downarrow}a_{3\downarrow} - \text{h.c.}\right)} \end{aligned} \tag{13}$$

Scenario II: Here we consider the quantum circuit design of Ref. 28 explicitly and illustrate co-designing the ansatz together with the set of rotations for the measurements. This strategy enables the measurement process to adapt to the specific state produced by the quantum register. Moreover, it takes advantage of the circuit structure for the Hamiltonian evaluations. In this instance we built a quantum circuit defined by a sequence of rotations U_{R_k} and double excitations $U_{C_{\{p,q\}}}(\theta) \equiv U_C(\varphi) = e^{-i\frac{\varphi}{2}\left(a^\dagger_{p\uparrow}a^\dagger_{p\downarrow}a_{q\downarrow}a_{q\uparrow} + \text{h.c.}\right)}$. This Multi-Graph Circuit was defined in 28.

The circuit is made by a sequence of gates which aims at catching all the correlation contributes among the atoms. In order to do that it leverages the graph structure, i.e., the nodes of the graph define the correlated orbitals and the edges define the strength of the interaction. The produced state will be an approximation of the true wavefunction, as is typical in VQE algorithms, but we can interpret the rotation operations as existing contributions inside the quantum state, reflecting its underlying structure.

We tested the method on three molecular systems, H_4, H_6 and H_8, all arranged both on a line, with a bond length of 1.5Å, and scattered in space. The line configuration is a common benchmark dataset for quantum algorithms and in previous work[28] they proved to be valid stand-ins for real molecular systems, such as conjugated pi-systems of carbon atoms. To broaden our analysis, we also considered free geometries which hold no structure. The bond length between the bonding and the dissociation distance makes the ground-state wavefunction not trivially simulable and not accurately representable as an HCB approximation. The sets of orbital rotation operations used are tailored to the graphs that can be defined by creating only paired connections between atoms. We defined 3, 5 and 6 graphs for H_4, H_6 and H_8 systems respectively. For scattered H_6 molecules we generated 50 additional unitary transformations randomly generated. The corresponding quantum gates in Jordan-Wigner encoding are:

$\mathscr{R} =$ 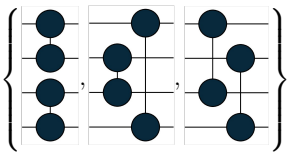 (14)

$\mathscr{R} =$ 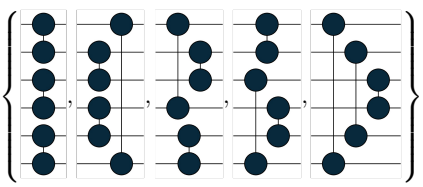 (15)

View Article Online
DOI: 10.1039/D5DD00251F

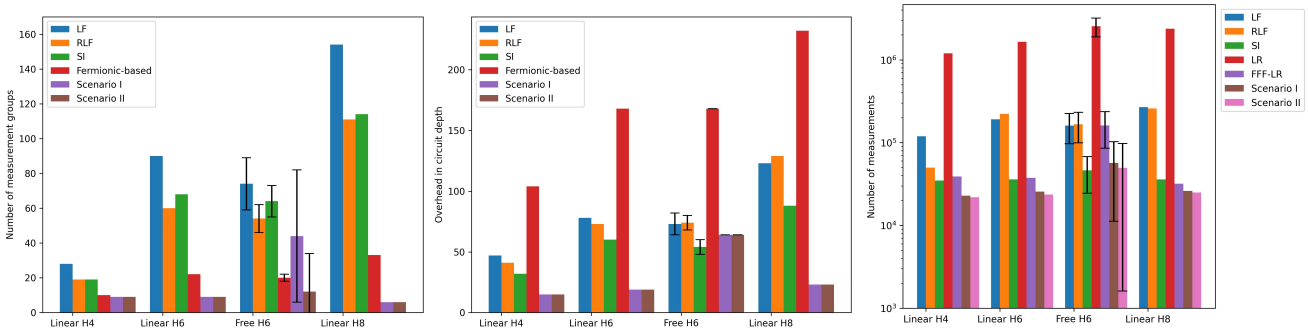

Fig. 2 (Left) Number of measurement groups needed for different reduction methods. Free H_6 refers to randomized molecular geometries, and the values correspond to the mean and standard deviation of the distribution that achieves an error below 2 mE_h. (Middle) Overhead in circuit depth given by the application of rotation operation on wavefunction in step 4. Here we considered only linear system examples since results are compatible. Values of Scenario I and II are expressed in the Reordered Jordan-Wigner encoding. (Right) Number of measurements required to compute all the contributions given by the general procedure. This represents the cost for each shot of a VQE algorithm.

$$\mathscr{R} = \left\{ \quad , \quad , \quad , \quad , \quad , \quad \right\} \tag{16}$$

using 8, 12 and 16 qubits respectively.

The topology of the rotation operations is derived from Valence-Bond Theory resonance structures. In particular, the number of structures available scales as $\frac{1}{n+1}\binom{2n}{n}$. These are the non-crossing perfect matching of n nodes in a ring. For H_4, H_6 and H_8 there are 2, 5 and 14 structures respectively. In the presented sets we considered one additional structure for H_4, operation number three, because the two structures alone were not able to catch all the relevant interactions in the molecule. We considered only 6 of the structures for H_8, for simplicity. The number of structures one can use scales fast but the used sets have proven to be effective for the target systems. This does not prevent the use of different topologies such as crossing edges or graphs with multiple pairs as long as the operations are well defined.

Figure 3 shows the error of the Hamiltonian approximation for each iteration. Figure 2 show the number of measurement groups and the depth overhead in the measuring circuits in comparison with grouping heuristics. When computing the depth of measuring circuits, the values for Scenario I and II are considered in the Reordered Jordan-Wigner encoding, meaning that the qubits order in the quantum register follows the pattern $|\uparrow\uparrow \ldots \uparrow\downarrow\downarrow \ldots \downarrow\rangle$. This choice leads us to a lower depth overhead by decoupling spin-up and spin-down excitations gates.

4.2 Numerical Results: Individual Shots

Given $H = \sum_i H_i = \sum_i w_i P_i$, for each Pauli string P_i we estimate the number of measurements as:

$$M_i = \left(\frac{|w_i| \sqrt{\mathrm{Var}(P_i)}}{\varepsilon} \right)^2 = \left(\frac{|w_i| \sqrt{(1 - \langle P_i \rangle_\Psi^2)}}{\varepsilon} \right)^2 \tag{17}$$

where $\varepsilon = 10^{-3}$ represents the precision.[14] Then, for each commuting group we only consider the largest value

$$M_{\mathrm{group}} = \max_{H_i \in \mathrm{group}} M_i, \tag{18}$$

since we can measure the operators belonging to such group simultaneously, therefore giving an upper bound on the total measurements for the given fragment. Finally, we sum together all the contributions from each iteration to retrieve the total number of measurements.

$$M_{\mathrm{tot}} = \sum_{\{\mathrm{groups}\}} M_{\mathrm{group}} \tag{19}$$

Figure 2 shows the number of measurements needed for a complete repetition of the procedure compared to grouping heuristics. These values have been proven consistent from the finite sample simulations in Figure 4. The number of samples was set to the estimated number of measurements, previously defined as the maximum value among all Pauli strings within the same group. We then repeated this process 100 times and computed the average over all sample simulations for each group. Our assumption is that the final result remains below the previously fixed precision $\varepsilon = 10^{-3}$ with respect to the real expectation value. In Scenario I and II the measurement groups are distributed and evaluated over each rotation operation, whereas for SI they are computed simultaneously. In all considered examples the error never exceeds the precision, thus confirming the consistency of the estimated number of measurements.

4.3 Scientific Software

All the calculations have been carried within the TEQUILA[30] PYTHON package. Specifically, the simulations made use of QULACS[31], the qubit operators elaboration utilized OPENFERMION[32], while the integral computations employed the PYSCF package[33] and the exact diagonalization SCIPY[34]. Finally, free geometries have been generated with QUANTI-GIN[35] and circuits depictions are made with QPIC[36].

View Article Online
DOI: 10.1039/D5DD00251F

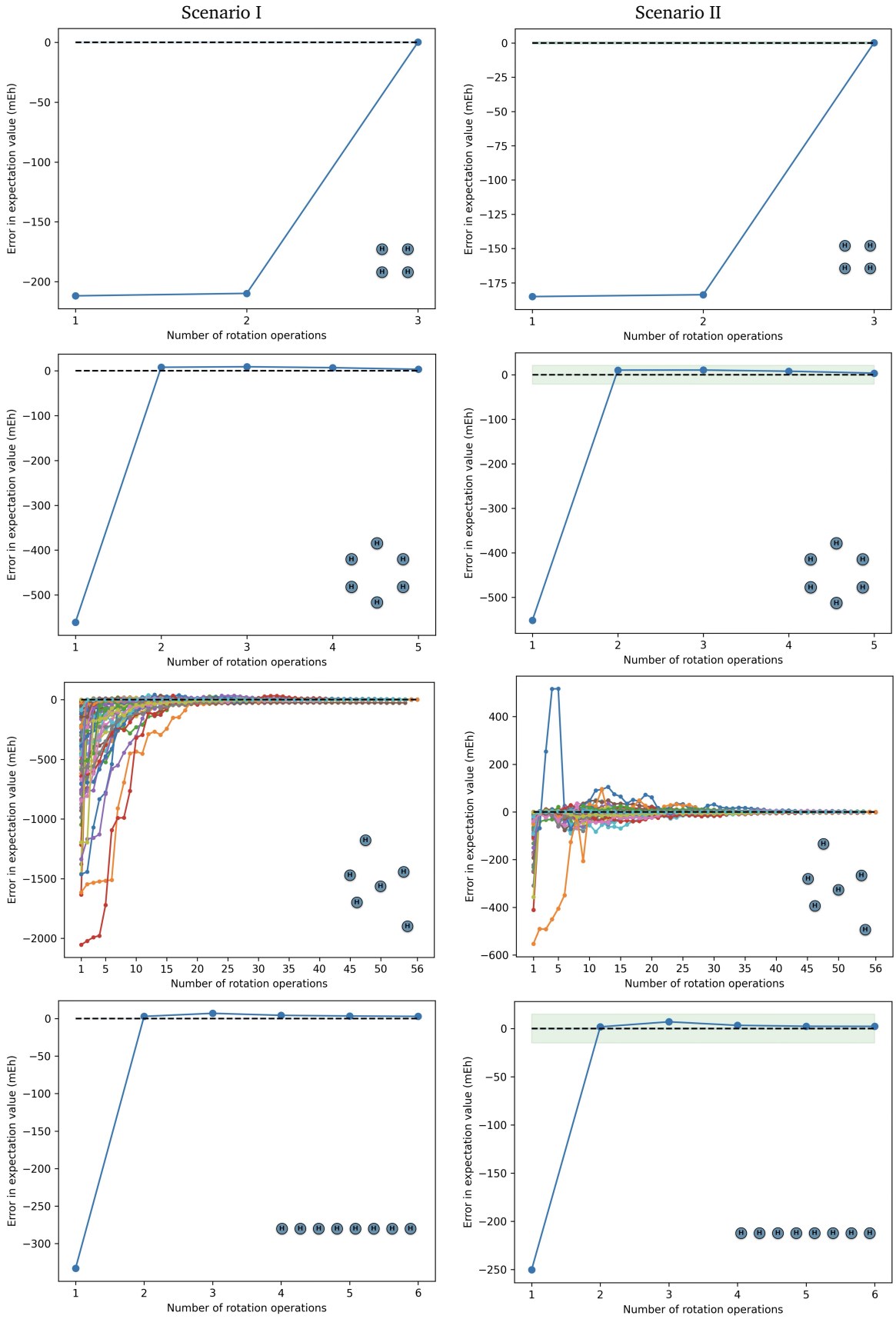

Fig. 3 Error in approximating the molecular Hamiltonian for square H_4, circular H_6 as well as free H_6 and linear H_8 using the sets $\{R_{G_k}\}$ from Eqs.(14), (15) and (16) respectively. The blue area is the 1 mE_h margin of error, which we consider as the desired accuracy, the green area is the error from the chosen circuit ansatz.

View Article Online
DOI: 10.1039/D5DD00251F

Table 1 Overview over the State-of-the-art methods used for the comparison with Scenario I and II in 2 with references.

Pauli-grouping	
Large First (LF)	11
Recursive Largest First (RLF)	11
Sorted Insertion (SI)	12,25
Fermionic-grouping	
Low-rank decomposition (LR)	14,15
Fluid Fermionic Fragments (FFF-LR)	16

5 Conclusion and Outlook

In all cases examined we consistently retrieved accurate approximations for the expectation value of the molecular Hamiltonian, achieving this with a comparably small number of iterations. Moreover, compared to existing approaches, our method does not rely on extensive pre-computation. The number of measurement groups is improved by 50% to 80% compared to benchmarks.[19] In Scenario II, 80% of the distribution falls under 10 measurement groups. The co-design of circuit and rotation operations may lead to more expressivity in the HCB Hamiltonian evaluation and thus fewer algorithm iterations needed, though this is not fully conclusive yet. Orbital rotation operations have shown to statistically improve this approximation at a cheap cost in circuit depth overhead, even when generated randomly. This work provides the ground to conduct further research to single out the optimal class of operations. Notably, the total number of measurements is lower by about 30% to 80% for structured systems, while comparable in magnitude to benchmarks for less-structured examples. The target systems have been proved to be well described by the graph-based approach introduced.[23,28] This agreement validates the efficacy of the proposed method, indicating the underlying principles are fundamental to the structural properties of these systems and supporting the hypothesis that the method can be systematically generalized to a broader range of systems. In the Appendix we show the example of the BeH_2 molecule for which we applied the same procedure as the linear H_4 molecule. The same reasoning can be applied by using circular H_6 to measure the benzene molecule. Future heuristics could leverage modern correlation measures[37–39] to enhance Hamiltonian approximation, or make use of perturbative methods[40,41] to narrow the choice of rotation operations with respect to expressivity and efficiency.

This approach has a connection to Fermionic quantum compute platforms. In Ref. 42 a randomized protocol has been developed that leverages rotations into different Fermionic basis – these operations are identical to the U_R operations used in this work, for this reason our heuristic protocol can be straightforwardly applied on such platforms with large improvements, e.g., the H_4 system required a few thousand basis rotations while the heuristic approach from this work requires only 3 rotations. The two approaches are two goalposts, a structural approach and a randomized zero-knowledge approach[42], that can be combined. In this work, we indicated it in Fig. 3 where we used a primitive randomized protocol. One can see the randomized protocol as an upper bound, a costly brute force attempt, and the structured scheme as a lower bound, a cheap structured attempt that can mitigate the high measurement costs as soon as structural information about the system is available.

Author contributions

DB: Writing (original draft), Formal Analysis, Methodology, Software, Data Curation, Visualization JSK: Conceptualization, Project Administration, Supervision, Funding Acquisition, Software, Writing (review and editing)

Conflicts of interest

There are no conflicts to declare.

Data availability

All data have been computed using the open-source library Tequila (v1.9.9).[30] A prototype implementation of the developed methods as well as data presented in the main text can be found under DOI:10.5281/zenodo.17607749.

Acknowledgements

This work has been funded by the German Federal Ministry of Research, Technology and Space (BMFTR, Quantum Technologies:HoliQC2).

Notes and references

1 A. Peruzzo, J. McClean, P. Shadbolt, M.-H. Yung, X.-Q. Zhou, P. J. Love, A. Aspuru-Guzik and J. L. O'brien, *Nature Communications*, 2014, **5**, 4213.
2 J. R. McClean, J. Romero, R. Babbush and A. Aspuru-Guzik, *New Journal of Physics*, 2016, **18**, 023023.
3 J. Tilly, H. Chen, S. Cao, D. Picozzi, K. Setia, Y. Li, E. Grant, L. Wossnig, I. Rungger, G. H. Booth and J. Tennyson, *Physics Reports*, 2022, **986**, 1–128.
4 A. Anand, P. Schleich, S. Alperin-Lea, P. W. K. Jensen, S. Sim, M. Díaz-Tinoco, J. S. Kottmann, M. Degroote, A. F. Izmaylov and A. Aspuru-Guzik, *Chemical Society Reviews*, 2022, **51**, 1659–1684.
5 K. Bharti, A. Cervera-Lierta, T. H. Kyaw, T. Haug, S. Alperin-Lea, A. Anand, M. Degroote, H. Heimonen, J. S. Kottmann, T. Menke, W.-K. Mok, S. Sim, L.-C. Kwek and A. Aspuru-Guzik, *Reviews of Modern Physics*, 2022, **94**, 015004.
6 M. Cerezo, A. Arrasmith, R. Babbush, S. C. Benjamin, S. Endo, K. Fujii, J. R. McClean, K. Mitarai, X. Yuan, L. Cincio, and P. J. Coles, *Nature Reviews Physics*, 2021, **3**, 625–644.
7 P. Schleich, J. S. Kottmann and A. Aspuru-Guzik, 2021.
8 F. Langkabel, S. Knecht and J. S. Kottmann, *The advent of fully variational quantum eigensolvers using a hybrid multiresolution approach*, 2024, `https://arxiv.org/abs/2410.19116`.
9 A. Aspuru-Guzik, A. D. Dutoi, P. J. Love and M. Head-Gordon, *Science (New York, N.Y.)*, 2005, **309**, 1704–1707.
10 J. F. Gonthier, M. D. Radin, C. Buda, E. J. Doskocil, C. M. Abuan and J. Romero, *Physical Review Research*, **4**, 033154.

View Article Online
DOI: 10.1039/D5DD00251F

Fig. 4 Finite samples simulation for three molecules: linear H_4, linear H_6 linear H_8. SI method is used as a benchmark. In Scenario I and II, the rotation operations and the measured groups correspond to those used for the approximation of Hamiltonian expectation values. As mentioned above we set a threshold precision of $\varepsilon = 10^{-3}$.

11 V. Verteletskyi, T.-C. Yen and A. F. Izmaylov, *Journal of Chemical Physics*, 2020, **152**, 124114.
12 Z. P. Bansingh, T.-C. Yen, P. D. Johnson and A. F. Izmaylov, **126**, 7007–7012.
13 T.-C. Yen, A. Ganeshram and A. F. Izmaylov, *npj Quantum Information*, **9**, 1–7.
14 W. J. Huggins, J. R. McClean, N. C. Rubin, Z. Jiang, N. Wiebe, K. B. Whaley and R. Babbush, *npj Quantum Information*, **7**, 1–9.
15 T.-C. Yen and A. F. Izmaylov, *PRX Quantum*, **2**, 040320.
16 S. Choi, I. Loaiza and A. F. Izmaylov, *Quantum*, **7**, 889.
17 G. García-Pérez, M. A. Rossi, B. Sokolov, F. Tacchino, P. K. Barkoutsos, G. Mazzola, I. Tavernelli and S. Maniscalco, *PRX Quantum*, 2021, **2**, 040342.
18 D. Miller, L. E. Fischer, K. Levi, E. J. Kuehnke, I. O. Sokolov, P. K. Barkoutsos, J. Eisert and I. Tavernelli, *npj Quantum Information*, 2024, **10**, 122.
19 A. Gresch, U. Tepe and M. Kliesch, *Arxiv:2502.01730*, 2025.
20 V. E. Elfving, M. Millaruelo, J. A. Gámez and C. Gogolin, *Physical Review A: Atomic, Molecular, and Optical Physics*, 2021, **103**, 032605.
21 J. S. Kottmann and F. Scala, *Journal of Chemical Theory and Computation*, 2024, **20**, 3514–3523.
22 L. Zhao, J. Goings, K. Shin, W. Kyoung, J. I. Fuks, J.-K. K. Rhee, Y. M. Rhee, K. Wright, J. Nguyen, J. Kim and S. Johri, *npj Quantum Information*, 2023, **9**, 60.
23 J. S. Kottmann and A. Aspuru-Guzik, *Physical Review A*, 2022, **105**, 032449.
24 F. J. del Arco Santos and J. S. Kottmann, *Quantum Science and Technology*, 2025, **10**, 035018.
25 O. Crawford, B. van Straaten, D. Wang, T. Parks, E. Campbell and S. Brierley, *arxiv:1908.06942*, 2019.

View Article Online
DOI: 10.1039/D5DD00251F

26 I. D. Kivlichan, J. McClean, N. Wiebe, C. Gidney, A. Aspuru-Guzik, G. K.-L. Chan and R. Babbush, *Physical Review Letters*, 2018, **120**, 110501.

27 Google AI Quantum and Collaborators, *Science (New York, N.Y.)*, 2020, **369**, 1084–1089.

28 J. S. Kottmann, *Quantum*, **7**, 1073.

29 *A Chemist's Guide to Valence Bond Theory*, John Wiley & Sons, Ltd, 2007, ch. 9, pp. 238–270.

30 J. S. Kottmann, S. Alperin-Lea, T. Tamayo-Mendoza, A. Cervera-Lierta, C. Lavigne, T.-C. Yen, V. Verteletskyi, P. Schleich, A. Anand, M. Degroote, S. Chaney, M. Kesibi, N. G. Curnow, B. Solo, G. Tsilimigkounakis, C. Zendejas-Morales, A. F. Izmaylov and A. Aspuru-Guzik, *Quantum Science and Technology*, 2021, **6**, 024009.

31 Y. Suzuki, Y. Kawase, Y. Masumura, Y. Hiraga, M. Nakadai, J. Chen, K. M. Nakanishi, K. Mitarai, R. Imai, S. Tamiya, T. Yamamoto, T. Yan, T. Kawakubo, Y. O. Nakagawa, Y. Ibe, Y. Zhang, H. Yamashita, H. Yoshimura, A. Hayashi and K. Fujii, *Quantum*, 2021, **5**, 559.

32 J. R. McClean, N. C. Rubin, K. J. Sung, I. D. Kivlichan, X. Bonet-Monroig, Y. Cao, C. Dai, E. S. Fried, C. Gidney, B. Gimby, P. Gokhale, T. Häner, T. Hardikar, V. Havlíček, O. Higgott, C. Huang, J. Izaac, Z. Jiang, X. Liu, S. McArdle, M. Neeley, T. O'Brien, B. O'Gorman, I. Ozfidan, M. D. Radin, J. Romero, N. P. D. Sawaya, B. Senjean, K. Setia, S. Sim, D. S. Steiger, M. Steudtner, Q. Sun, W. Sun, D. Wang, F. Zhang and R. Babbush, *Quantum Science and Technology*, 2020.

33 Q. Sun, T. C. Berkelbach, N. S. Blunt, G. H. Booth, S. Guo, Z. Li, J. Liu, J. D. McClain, E. R. Sayfutyarova, S. Sharma, S. Wouters and G. K.-L. Chan, *Wiley Interdiscip. Rev. Comput. Mol. Sci.*, 2018, **8**, e1340.

34 P. Virtanen, R. Gommers, T. E. Oliphant, M. Haberland, T. Reddy, D. Cournapeau, E. Burovski, P. Peterson, W. Weckesser, J. Bright, S. J. van der Walt, M. Brett, J. Wilson, K. Jarrod Millman, N. Mayorov, A. R. J. Nelson, E. Jones, R. Kern, E. Larson, CJ. Carey, İ. Polat, Y. Feng, E. W. Moore, J. Vand erPlas, D. Laxalde, J. Perktold, R. Cimrman, I. Henriksen, E. A. Quintero, C. R. Harris, A. M. Archibald, A. H. Ribeiro, F. Pedregosa, P. van Mulbregt and S. . . Contributors, *Nature Methods*, 2020, **17**, 261–272.

35 K. Stein, *Nylser/Quanti-Gin*, 2024, `https://github.com/nylser/quanti-gin`.

36 T. G. Draper and S. A. Kutin, *Qpic/Qpic*, qpic, 2025, `https://github.com/qpic`.

37 L. Ding, S. Mardazad, S. Das, S. Szalay, U. Schollwöck, Z. Zimborás and C. Schilling, *Journal of Chemical Theory and Computation*, 2021, **17**, 79–95.

38 L. Ding, S. Knecht, Z. Zimborás and C. Schilling, *Quantum Science and Technology*, 2022, **8**, 015015.

39 L. Ding, S. Knecht and C. Schilling, *The Journal of Physical Chemistry Letters*, 2023, **14**, 11022–11029.

40 L. Reascos, G. F. Diotallevi and M. Benito, *Arxiv:2411.11535*, 2024.

41 G. F. Diotallevi, L. Reascos and M. Benito, *arXiv:2412.10240*, 2024.

42 P. Naldesi, A. Elben, A. Minguzzi, D. Clément, P. Zoller and B. Vermersch, *Physical Review Letters*, 2023, **131**, 060601.

View Article Online
DOI: 10.1039/D5DD00251F

Appendix

Close-up visualization

Figure 6 display close-up visualizations of the approximation figures, i.e., the errors in approximating the molecular Hamiltonian operators of the selected examples.

Multiple atomic distances

Figure 9 shows the error measured for the linear H_4 with respect to interatomic distance. We can see that for short distances the chosen rotation operations behave poorly. A possible explanation for this result is that the operations defined through Valence-Bond Theory transform the orbital basis in a localized basis. This process makes it not accurate for situations where atoms are close together, whereas a delocalized basis, e.g., canonical orbitals, can prove more suitable. This behaviour can be observed in the simulation of randomized H_6 geometries where we noticed that the original set of operations alone is not enough to retrieve the full Hamiltonian. The solution adopted in that context, i.e., adding randomly generated unitary transformations, can be transferred to this system as well, even if the resulting measurement process becomes more expensive. Note however that this is significantly beyond the number of orbital rotations form comparable methods applied to the same system.[42]

Scenario II quantum circuit

The quantum circuit used in Scenario II is taken from[28]. It is made of a sequence of rotation (U_R) and correlation (U_C) gates. For example, the circuit used for linear H_6 is

$$\begin{aligned}|\Psi\rangle =& \tilde{U}^{\dagger}_{R_{G_4}}(\phi_4)U_{C_{G_4}}(\varphi_4)\tilde{U}_{R_{G_4}}(\phi_4)\\ & \tilde{U}^{\dagger}_{R_{G_3}}(\phi_3)U_{C_{G_3}}(\varphi_3)\tilde{U}_{R_{G_3}}(\phi_3)\\ & \tilde{U}^{\dagger}_{R_{G_2}}(\phi_2)U_{C_{G_2}}(\varphi_2)\tilde{U}_{R_{G_2}}(\phi_2)\\ & \tilde{U}^{\dagger}_{R_{G_1}}(\phi_1)U_{\mathrm{SPA}}(\varphi_1)|0\rangle\end{aligned} \tag{20}$$

where $U_{\mathrm{SPA}}(\varphi_1)$ is equivalent to $U_{C_{G_1}}(\varphi_1)\tilde{U}_{R_{G_1}}(\phi_1)$ since applying a rotation operation at the beginning of the circuit has no effect on the initial state. Figure 5 presents the circuit rendered with QPIC. In this context $\tilde{U}_{R_k} = U_{R_k}U_{RR}$ is an extension of the orbital rotation operation which preserves the topology and allows delocalization. The definition of U_{RR} is based on Eq.(28) of Ref. 28. The parameters for the $\tilde{U}_{R_k}$ gates are initialized through the GNM method from Ref. 21 and then the whole is minimized. We show an example code to create the circuit for linear H_6 in 1.

BeH_2 molecule and method scaling

In order to assess the scaling of the method we applied it on the BeH_2 molecule. The results are shown in Figure 10. The orbital rotation operations are the same as the linear H_4 molecule and the accuracy comparably high. We didn't consider the p_x and p_y orbitals, but only the s and p_z ones. This makes it suitable for the linear H_4 graph topology. The example shows how the heuristic can be extended on larger molecules by applying the same orbital rotation operations to molecules with the same topology. A similar example is the application of the operations of linear H_6 over the benzene molecule. In addition one can consider the discarded orbitals using a mixed Fermionic-Bosonic encoding[24] to obtain a complete description of the system.

Excited state calculation

The measurement protocol can be extended to excited state calculation. In order to prove this we considered the five lowest Hamiltonian eigenvector states with $\langle S^2\rangle = 0$ and energy higher than the ground state. The procedure is unchanged, the rotation operations are the same as used for the ground state computation. The result is shown in Figure 11.

```python
import tequila as tq

# Create the H6 molecule
geom = "h 0.0 0.0 0.0\nh 0.0 0.0 1.5\nh 0.0 0.0 3.0\nh 0.0 0.0 4.5\nh 0.0 0.0 6.0\nh 0.0 0.0 7.5"
mol = tq.Molecule(geometry=geom, basis_set="sto-3g").use_native_orbitals()

# Convenience method for URR
def URR(layer):
    return mol.UR(0,1,("01a",layer)) + mol.UR(2,3,("23a",layer)) + mol.UR(4,5,("45a", layer)) \
         + mol.UR(0,3,("03a",layer)) + mol.UR(1,2,("12a",layer)) \
         + mol.UR(0,1,("01b",layer)) + mol.UR(2,3,("23b",layer)) + mol.UR(4,5,("45b", layer)) \
         + mol.UR(0,3,("03b",layer)) + mol.UR(1,2,("12b",layer)) \
         + mol.UR(0,1,("01c",layer)) + mol.UR(2,3,("23c",layer)) + mol.UR(4,5,("45c", layer))

# First layer
U = mol.make_ansatz("spa", edges=[(0,1),(2,3),(4,5)])
U+= (mol.UR(0,1,"01") + mol.UR(2,3,"23") + mol.UR(4,5,"45") + URR(0)).dagger()

# Second layer
U+= mol.UR(0,5,"05") + mol.UR(1,2,"12") + mol.UR(3,4,"34") + URR(1)
U+= mol.UC(0,5,"05") + mol.UC(1,2,"12") + mol.UC(3,4,"34")
U+= (mol.UR(0,5,"05") + mol.UR(1,2,"12") + mol.UR(3,4,"34") + URR(1)).dagger()
```

Listing 1 How to prepare a quantum circuit in tequila

View Article Online
DOI: 10.1039/D5DD00251F

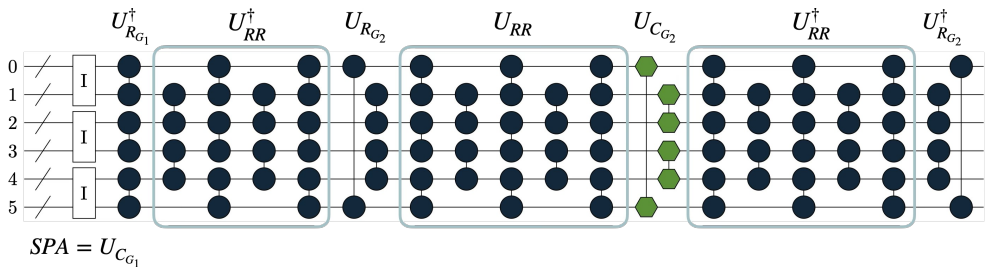

Fig. 5 Quantum circuit used in Scenario II for linear H_6 molecule.

View Article Online
DOI: 10.1039/D5DD00251F

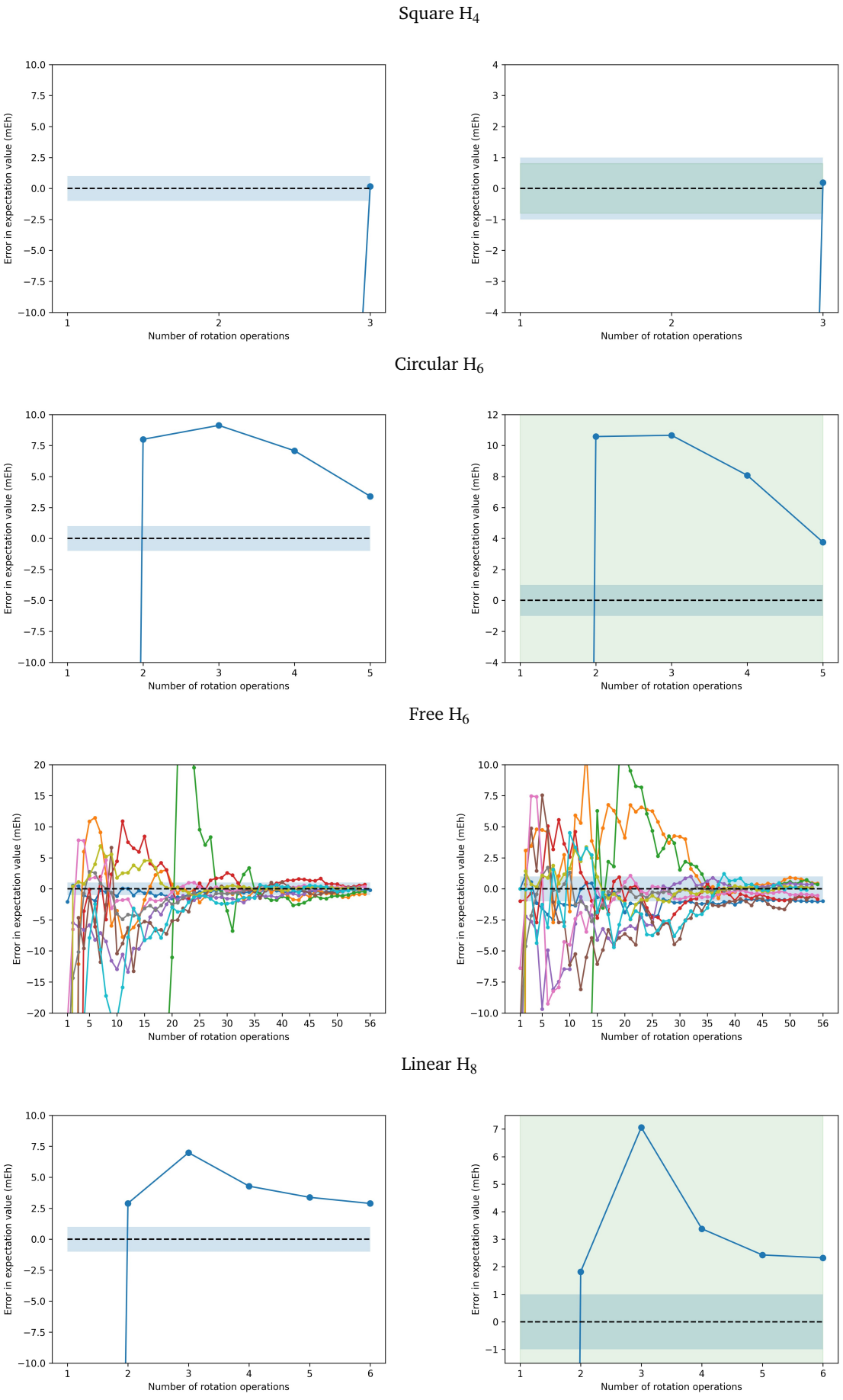

Fig. 6 Close-up visualization of Figure 3. The blue area is the 1 mE_h margin of error, which we consider as the desired accuracy, the green area is the error from the chosen circuit ansatz.

View Article Online
DOI: 10.1039/D5DD00251F

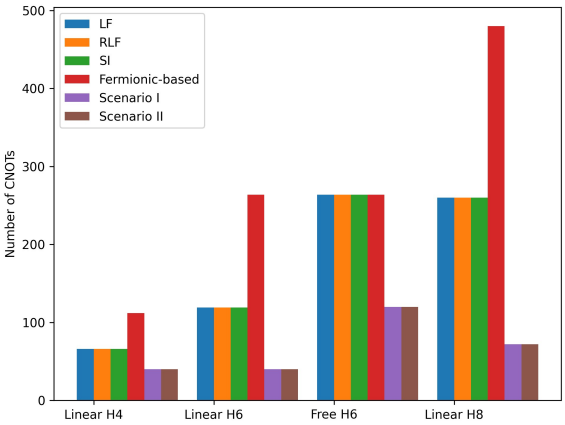

Fig. 7 Number of CNOT gates in the circuit used for the rotation operation in step 4, compared to CNOT counts for the basis transformation for grouping approaches. The results are consistent with the circuit depths in the main paper and show an improvement of the new method over state-of-art ones.

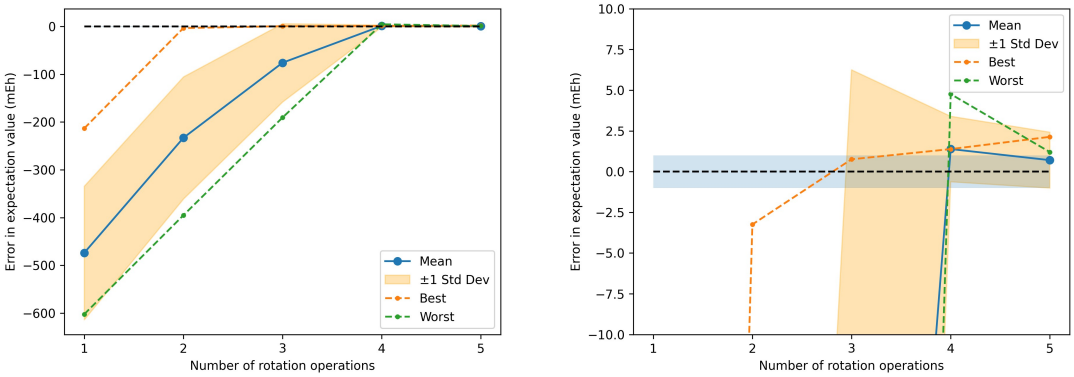

Fig. 8 Error in approximating the molecular Hamiltonian of linear H_6 molecule for all possible orderings of the rotation operations in the set. The worst result is obtained for sequence (5,2,3,4,1), while best corresponds to sequence (1,2,3,4,5), i.e., the one used in the work. (Left) Full plot. (Right) Close-up visualization. The standard ordering shows up to return the best result in the least number of steps. An explanation is that the first graph has the minimum sum of the lengths of the edges, the second has the second least sum of the lengths and so on, and thus they catch the correlation between the atomic orbitals in less steps. Nevertheless, every ordering reaches the best accuracy (1 mEh) given enough steps. This is a first indication that the defined set of rotation operations is overall sufficient to catch the correlations between the atomic orbitals.

View Article Online
DOI: 10.1039/D5DD00251F

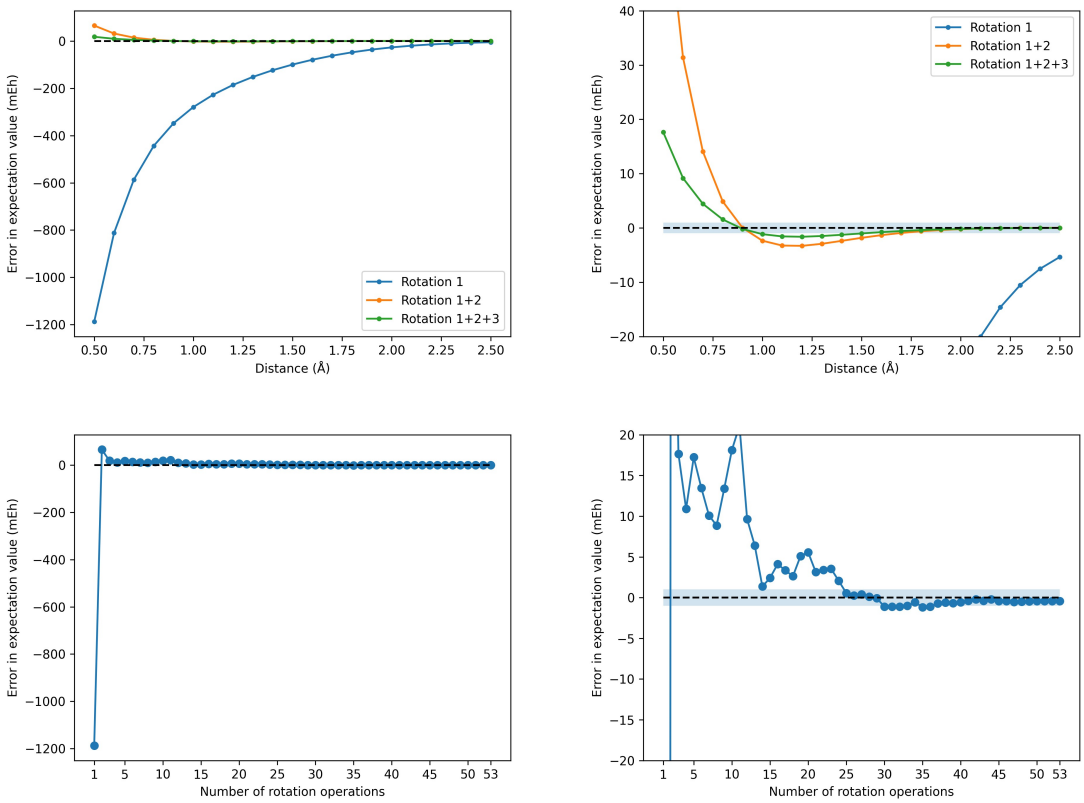

Fig. 9 Error in approximating the molecular Hamiltonian of linear H_4 molecule. (Top) We considered multiple atomic distances and only the standard set of rotation operations for the H_4 molecule. (Bottom) We considered only 0.5Å atomic distance and on top of the standard set we added 50 randomly generated unitaries as rotation operations, in the same manner as with H_6 molecules in random geometries (Figure 3). For further explanation see Appendix.

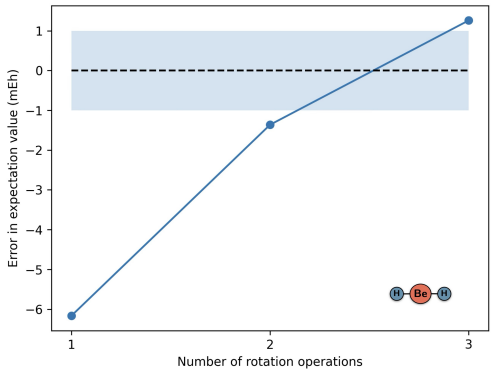

Fig. 10 Error in approximating the molecular Hamiltonian of BeH_2 molecule with a bond distance of 1.5Å in Scenario I. This shows that the heuristic can be extended on larger molecules with the same topology by applying the same orbital rotation operations.

View Article Online
DOI: 10.1039/D5DD00251F

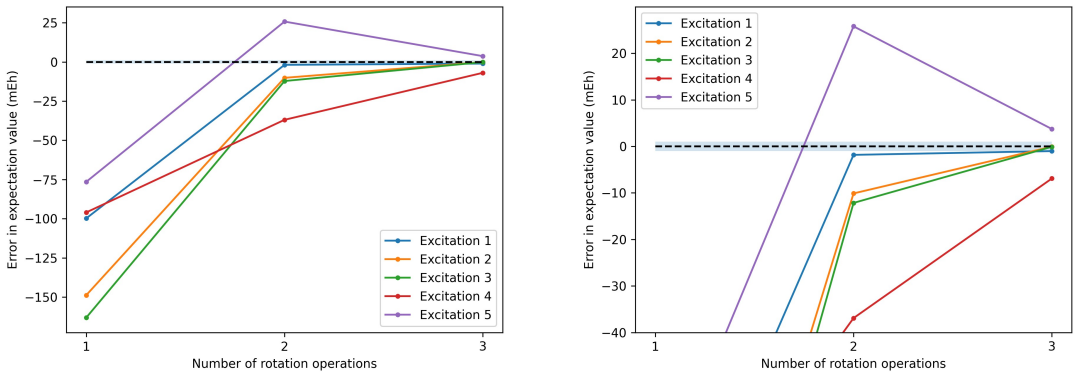

Fig. 11 Error in approximating the molecular Hamiltonian of linear H_4 molecule for the first five excited states. (Left) Full plot. (Right) Close-up visualization. This shows that the process is not limited to computation of ground state expectation value but can be extended to arbitrary many-body states.

All data have been computed using the open-source library Tequila (v.1.9.9, DOI:10.5281/zenodo.7673865.).
A prototype implementation of the developed methods as well as data presented in the main text can be found under DOI:10.5281/zenodo.17607749

View Article Online
DOI: 10.1039/D5DD00251F